Research Article

Advances in Mechanical Engineering

Advances in Mechanical Engineering
2021, Vol. 13(4) 1–15

DOI: 10.1177/16878140211011888
journals.sagepub.com/home/ade
SAGE

Bentonite-based composites with ceramic and metallic powders additions for use as filters

Simona Matei, Maria Stoicanescu, Varga Bela, Elena Tiron and Aurel Crisan

Abstract

This paper represents the study of bentonite matrix composite reinforced with ceramic (Al_2O_3 and SiC) and metallic (Al and Fe) particles for the production of filters. Ceramic powders were used to generate pores and metallic particles to control the pore size (to finish them). These materials were added to composites in two stages. In the first stage, the ceramic particles (Al_2O_3 and SiC) were added to the bentonite matrix, thus obtaining two types of composites. In the second stage, for each type of composite, metallic powders of Al and Fe were added. The composites was prepared by mixing the components, cold pressing for compaction in cylindrical samples and, at the end, sintering at 1250°C. The samples thus produced underwent studies by optical and electron microscopy, diffractometry, dilatometry and thermal analysis and tests to determine the compressive strength and the porosity. Thus, there was obtained useful information regarding the behaviour and impact of the reinforcing materials in the process of producing the composites, and on their impact on the final properties of the composites produced.

Keywords

Ceramic composites, bentonite, thermal analysis, metallic particles, ceramic filters

Date received: 11 November 2020; accepted: 29 March 2021

Handling Editor: James Baldwin

Introduction

Composites of ceramic materials can be made using a multitude of aggregation materials (Al_2O_3, SiO_2, SiC, ZrO) and consolidation materials (clays, cement).[1–3] They are used in a very wide range of products and domains, some of the most interesting being ceramic filters. Silicon carbide (SiC) and silicon oxide (SiO_2) are the most used materials for the manufacture of ceramic filters due to its high corrosion resistance, thermal shock resistance and excellent mechanical strength.[3–9] From these composites can be obtained filters with high porosity, fine pore distribution and resistance in chemically aggressive environments or at high temperatures, according to the intended use.[10–12]

The processes for obtaining ceramic filters also vary greatly: by compacting single-fraction powders,[13–16] by casting,[17,18] by the sol-gel method.[19,20] For example, those based on silicon carbide can be produced by: casting slip,[21,22] vacuum extrusion,[23] melt infiltration,[24] etc. Uddin[25] employed the extrusion technique to prepare supports for pyrophyllite ceramic membranes, used for microfiltration applications. For ultrafiltration and microfiltration applications, Bouzerara et al.[26] used a mixture of dolomite and kaolin, Mamoudi et al.[27] used natural apatite, Saffaj et al.[28–30] used natural Moroccan

The Material Science Department, Transilvania University of Brasov, Braşov, Romania

Corresponding author:
Simona Matei, The Material Science Department, Transilvania University of Brasov, B-dul Eroilor, Nr. 29, Braşov 500036, Romania.
Email: simona.matei@unitbv.ro

clay and cordierite, Archiou et al.[31] used natural Moroccan pozzolan. Şan et al.[32] have recently produced ceramic filters from a cheap mixture of ceramic powders (quartz, zeolite and frit glass) and the material produced had superior properties. These filters were produced by slip casting and pressing.[32] The obtaining and use of ceramics are accompanied by the appearance of specific defects such as: surface or volume cracks that can substantially change their behaviour.[2]

The addition of metallic particles in ceramic composites can modify both their properties and their behaviour in processing and use.[33] Depending on the preparation method, the addition of metallic particles can determine the occurrence in situ of specific phases (as in the case of the present study) that have an important role on their properties.

Clay-based ceramic materials are used in metallurgy, mechanical engineering and the chemical industry as refractory materials, filter and catalyst materials,[34,35] in applications for bacteria removal (microfiltration), virus and colloid removal (ultrafiltration) and dissolved organic matter removal (nanofiltration), for desalination and for the production of ultrapure water.[36,37]

Clays, especially bentonite, are of interest for research due to their absorption properties and high porosity.[38] These materials are very inexpensive and they can be easily sourced from several regions.

Bentonites are a variety of clays with a high content of montmorillonite (over 70%).[39] Due to the high adsorption of water and to the ion exchange, bentonite can be used in various technological applications, for example, catalysts in the chemical processing, additives for plasticizing and manipulating the viscosity of ceramic pastes or sealing materials.[39] Compacted bentonite is characterized by low permeability, long-term stability, high self-sealing and adsorption capacity.[39] It is used at all times to increase plasticity in ceramic bodies.

The aim of this research is to obtain bentonite-based composites with the addition of ceramic particles (SiC and Al_2O_3) that have the role of ensuring the necessary porosity of the material. From previous studies such materials have pore sizes dependent on the size of ceramic particles and their proportion in the mixture.[4–7] The uniformity of the pore is lower as the pore size is smaller. For very small pores (nano size), complex methods of manufacturing composites are recommended: a sol-gel process,[40] a solid-gas reaction[41] and a nanocasting process.[42] As a new method (simpler and efficient from a technological and economically point of view), we propose in this research the control of pore size by adding metal powders in composites. During sintering in the oven atmosphere the metal particles are transformed into compounds (oxides and combinations of oxides). These 'in situ' processes have important effects on the mechanical characteristics, size and shape of the pores, respectively the general porosity of the composite material. We specify that this procedure was not found in the researched literature.

Materials and methods

For the matrix, there was used Romanian bentonite from the Şuncuiuş area (53% montmorillonite $(Na,Ca)_{0.33}(Al,Mg)_2(Si_4O_{10})(OH)_2 \cdot nH_2O$; 1.3% Fe_2O_3; 45.7% SiO_2). For reinforcement, there were used Al_2O_3 (50 μm grain size) and SiC (63–80 μm grain size) powders and metal powder additions of Al (<65 μm grain size) and Fe (<100 μm grain size). Bentonite was first mixed with SiC and with Al_2O_3, respectively, in proportions of 40/60 wt%, thus obtaining two groups of materials. These were mixed for homogenization with a 12 wt% addition of water for a total of 20 min. There were added to each of these two groups of compositions amounts of Al and Fe powders between 5 and 17 wt%, mixing until complete homogenization. A household electric mixer (max. 1 kg capacity) was used for mixing. Table 1 shows the proportions of the components used to produce the samples.

The mixtures produced were cold pressed at 20 kN for compaction in cylindrical samples and then sintered at 1250 °C (60 min holding at this temperature), in the oven atmosphere. Cylindrical specimens with a diameter between 15 and 16 mm and a height between 11 and 15 mm were made using this method. In order to know the behaviour of the materials during their processing, dilatometry studies and differential thermal analyses were performed on different compositions. The cylindrical specimens produced underwent the following types of characterization: surface study by optical and electron microscopy, dilatometric analysis, thermal analysis, diffractometric analysis, determination of the mechanical properties and of the porosity.

The dilatometric analysis was performed using the horizontal dilatometer L75PT/1400°C. It allows the study of phase transformations in the solid state for the sample with thickness between 0.1 and 5 mm, with a maximum diameter of 6 mm, a temperature range of between 20°C and 1400°C, at a resolution of 0.125 nm/digit.

The differential thermal analysis was conducted using the thermal analyser NETZSCH STA 449 F3 JUPITER, TG/DTA type, with a heating rate of 10°C/min, from ambient temperature up to 900°C in a nitrogen atmosphere, with a flow rate of 20 ml/min in an alumina crucible.

The analysis of the surface by optical microscopy was conducted using the HIROX RH-2000 digital 3D microscope, on sintered samples in the oven atmosphere. As the sintering was carried out in the atmosphere, the metal particles were completely oxidized in

Table 1. Types of composites produced and the properties there of.

Sample no.	Components (wt %)				
	Bentonite	SiC	Al_2O_3	Al	Fe
3.1.1.	40	60			
3.1.1.1.Fe	38	57			5
3.1.1.1.Al	38	57		5	
3.1.1.2.Fe	36	55			9
3.1.1.2.Al	36	55		9	
3.1.1.3.Fe	35	52			13
3.1.1.3.Al	35	52		13	
3.1.1.4.Al	33	50		17	
3.2.1.	40		60		
3.2.1.1.Fe	38		57		5
3.2.1.1.Al	38		57	5	
3.2.1.2.Fe	36		55		9
3.2.1.2.Al	36		55	9	
3.2.1.3.Fe	35		52		13
3.2.1.3.Al	35		52	13	
3.2.1.4.Fe	33		50		17
3.2.1.4.Al	33		50	17	

the sample surface. It includes an ultra-fast autofocus and multifocal system, an integrated stepping motor with *Z*-axis movements of 50 nm per step and a motorized rotary head, which offers 360° rotation around the examined specimen. It enables real-time, accurate and calibrated measurements of length, angle, diameter and area, as well as powerful 3D software with surface topography and roughness measurements.

Micrographs were obtained using SEM, Hitachi, S3400N, type II equipment and the elementary quantitative analysis of the samples was performed using EDX (NSS model, 2,000,000 counts/s), with a sensitivity of up to several atomic percentages.

Mineralogical composition of bentonite was determined by X-ray diffraction (XRD) analysis. The diffractometric analysis was performed to find out if finally (after sintering) there are still metal particles in the composites. This one was performed using the D8 Advance Bruker diffractometer, with Cr anode used at 35 kV and 45 mA with a radiant wave $x = 2.28970$ Å. The detector is LYNXEYE_XE_T (1D mode) with detector opening 2.945°, lower discriminator 0.554 V, upper discriminator 0.604 V and detector profile Cr_HighResolution. The identification of the compounds was done using the online COD database (Crystallography Open Database).

The compressive strengths of the composites produced were determined on the universal machine for mechanical tests WDW-150S. This allows determinations and tests on non-standardized samples of mechanical properties, for a very wide temperature range (from −150°C to 1250°C). The test force is between 1 and 150 kN.

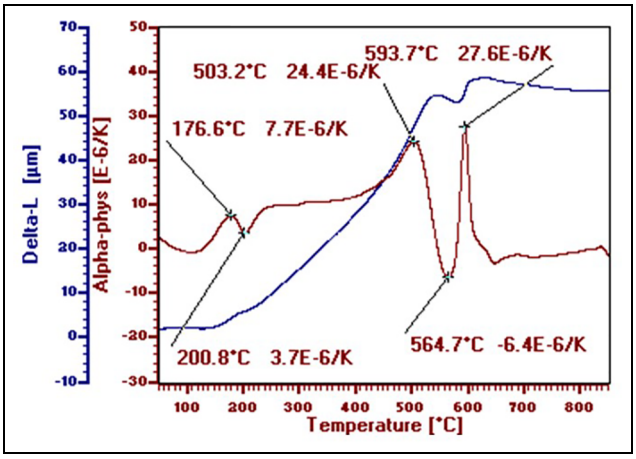

Figure 1. Thermal expansion curves for bentonites.

Experimental results

It is known that a number of heat induced transformations, accompanied by dimensional variations, occur in bentonites. The precise knowledge and evaluation there of is necessary in order to establish correct procedures for processing bentonite-based materials. It is also important to know the effects of some additives (ceramic and metallic powders in this case) on these transformations in order to obtain final products without defects and with appropriate properties. In order to meet these requirements, dilatometry determinations and differential thermal analyses were performed on both bentonite and certain compositions used in the study.

The dilatometric analysis

Figure 1 shows the dilatometric curves for bentonite. There can be seen significant variations of the coefficient of linear expansion in the zone of the temperatures at which significant transformations in the material occur, as also highlighted by the differential thermal analysis:

- Between 200°C and 300°C
- Between 500°C and 600°C.

As a whole, there can be seen a significant linear variation occurring before 600°C, after which the material is relatively stable dimensionally. This behaviour indicates that it is not recommended to add in the bentonite materials that determine the development of processes (chemical reactions, phase transformations) accompanied by volume increases during this thermal interval. During sintering, such volume increases can cause internal stresses, accompanied by significant dimensional

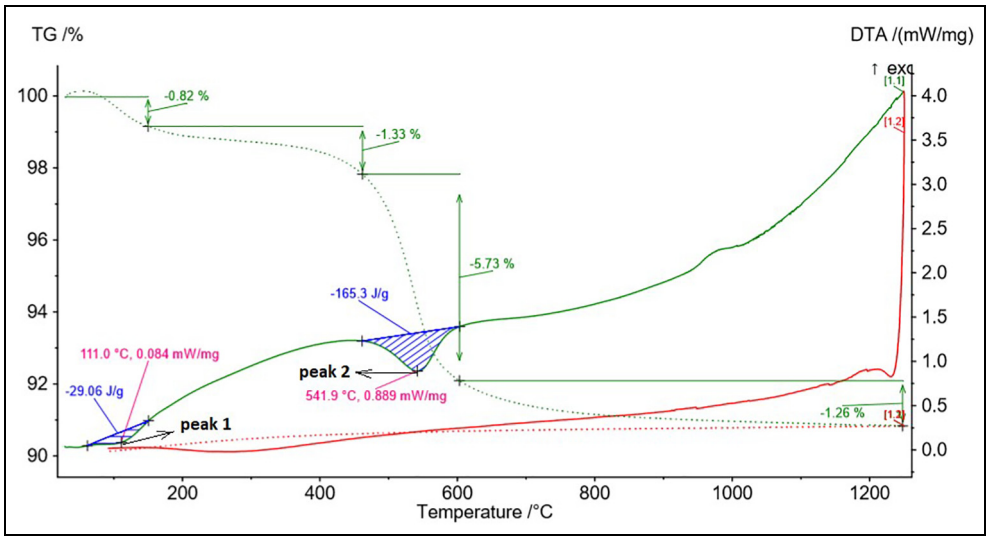

Figure 2. TG-DTA graph for bentonite.

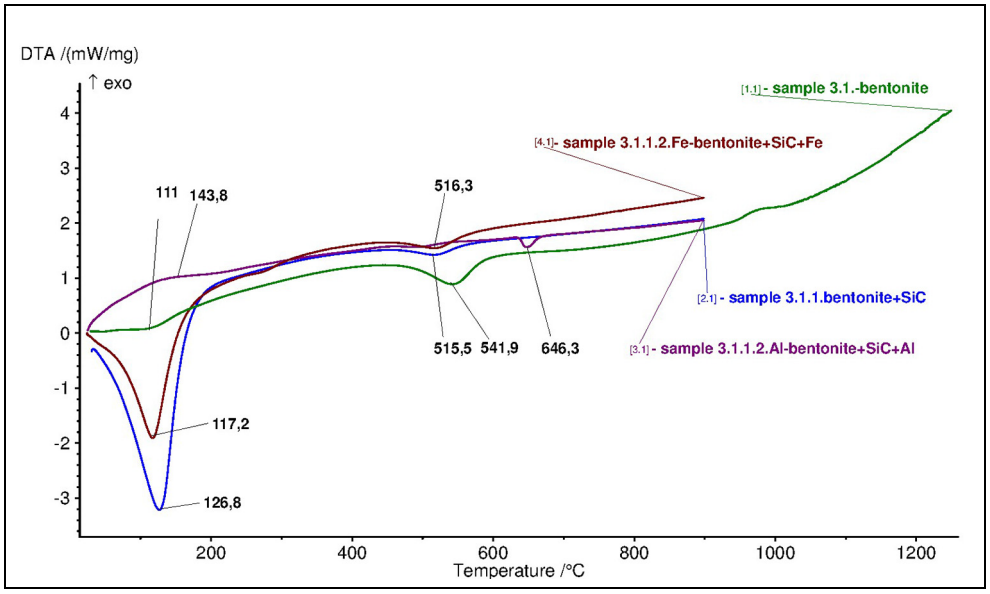

Figure 3. The appearance of DTA curves for composites with SiC, Fe and Al particle additions.

variations and by the occurrence of cracks and deterioration of materials.

The differential thermal analysis

The thermal analysis graphs indicate the temperatures at which significant transformations occur in terms of thermal effects and the mass variations for the analysed materials. Figure 2 shows the thermal analysis diagram for bentonite. There can be noted the existence of specific transformations:

- Between 80°C and 200°C – bentonite dehydrates, accompanied by an endothermic thermal effect and a matching loss of mass. The extreme value of this transformation is noted below as Peak 1;

- Between 500°C and 600°C – chemically bound water is lost, accompanied by the transformation of kaolinite into metacaolinite according to the reaction:[28]

$$2SiO_2 \cdot Al_2O_3 \cdot 2H_2O \rightarrow 2SiO_2 \cdot Al_2O_3 + 2H_2O, \quad (1)$$

This type of transformation is noted below as Peak 2.

The effect of introducing ceramic and metallic particles on these transformations was tracked for the composite materials produced. Figure 3 shows DTA curves for materials produced with SiC, Al and Fe additives in bentonite, and Figure 4 shows DTA curves for

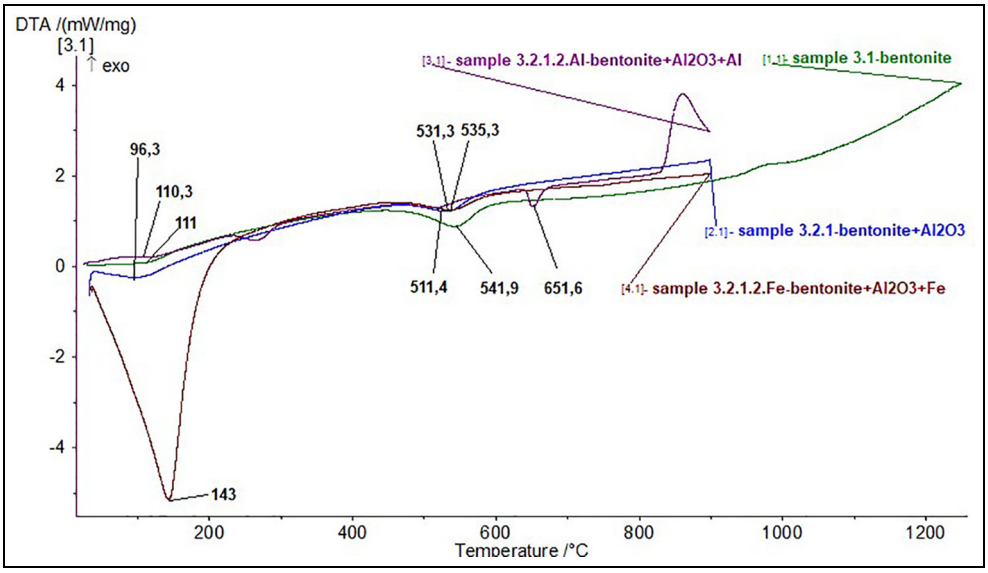

Figure 4. The appearance of curves for composites with Al_2O_3, Al and Fe particle additions.

Table 2. Specific values of the transformations for Peak 1 and Peak 2 of the composites.

Item	Sample no.	Peak 1			Peak 2			Total mass loss, %
		Temperature, °C	Specific energy, J/g	Mass loss, %	Temperature, °C	Specific energy, J/g	Mass loss, %	
1.	3.1.	111	−29.6	−0.82	541.9	−165.3	−1.33	−9.14
2.	3.1.1.	126.8	−698.5	−14.06	515.5	−19.87	−1.99	−17.93
3.	3.1.1.2.Fe	117.2	−383.9	−7.48	516.3	−46.13	−1.91	−12
4.	3.1.1.2.Al	143.8	27.95	−0.25	646.3	−17.72	−0.03	−2.69
5.	3.2.1.	96.3	−36.75	−0.63	531.3	−38.39	−2.78	−5.97
6.	3.2.1.2.Fe	143	−1351	−20.42	535.3	−26.51	−2.74	−26.64
7	3.2.1.2.Al	110.3	−0.5741	−0.46	511.4	−13.06	−1.29	−6.08

materials produced with Al_2O_3, Al and Fe additions in bentonite.

By adding SiC and Al_2O_3 ceramic powders, the nature of the composite transformations does not change. However, an increase of the endothermic effects at Peak 1 is observed in the case of SiC, compared with a negligible influence in the case of Al_2O_3. For the transformations in the Peak 2 zone, the effects are insignificant for each of the two types of ceramic powders added. This indicates that SiC is chemically active in the context of the processes occurring in bentonite during sintering.

The Al addition determines important changes due to its high reactivity in relation to the materials it comes into contact with. Being very active in relation to water vapours, it can oxidize when the mechanically bound water in bentonite is removed. Therefore, the Peak 1 transformation becomes exothermic. For Peak 2, the Al induced effect is insignificant. At 646.3°C (in the case of the bentonite and SiC mixture) and of 651.6°C (in the case of the bentonite and Al_2O_3 mixture), there occurs an endothermic transformation, which is the melting of the Al particles. The lower value of this temperature in the case of SiC is determined by the diffusion of Si from SiC into the metal particles of Al (the temperatures and the small dimensions of the materials favour this process), so that their composition moves to that of the eutectic from the Al-Si system, with melting temperature at 577°C.

The addition of Fe in these materials strongly accentuates the endothermic effect of the associated transformation for Peak 1, more for the bentonite + Al_2O_3 mixture than for bentonite + SiC (see Figure 4 compared with Figure 3). The tracking of the mass losses associated with these transformations, shown in Table 2, reveals that they have the same dependence on the presence of iron as the thermal effects of the transformations (the specific energy at the transformation).

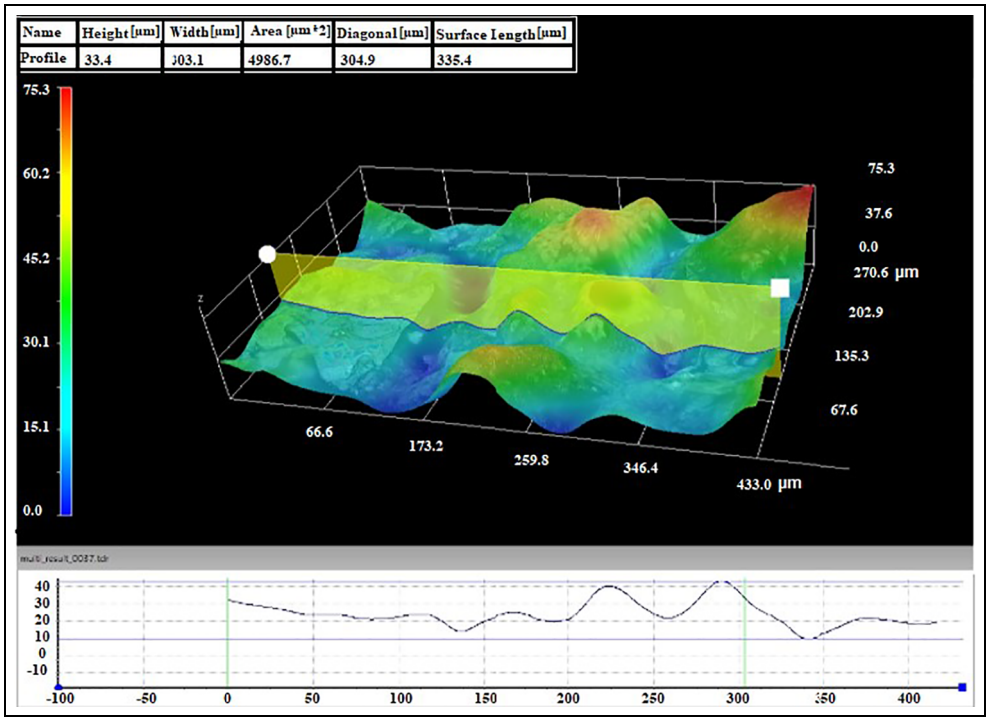

Figure 5. Surface profile for the composite with bentonite matrix reinforced with SiC and Al particles.

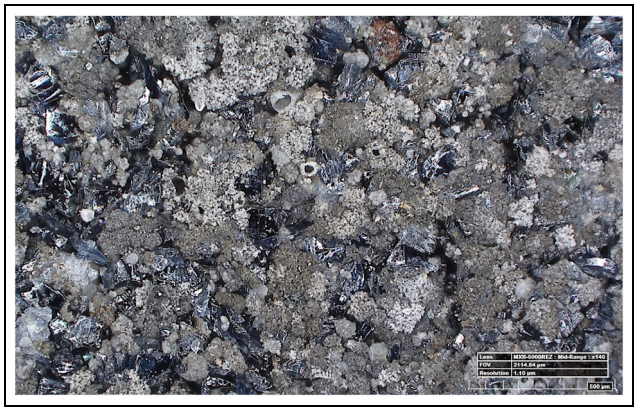

Figure 6. Surface appearance for the composite with bentonite matrix reinforced with SiC and Al particles.

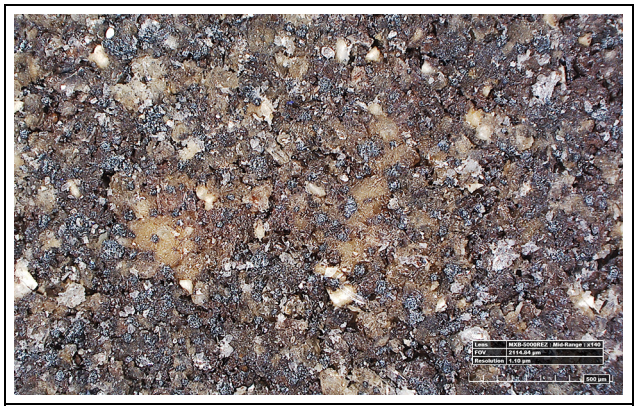

Figure 7. Surface appearance for the composite with bentonite matrix reinforced with Al_2O_3 and Fe particles.

This proves that the presence of Fe determines a lower conservation in the materials of the water used to make the mixture, during their processing and consequently an accentuation of the dehydration process associated with the temperature range for Peak 1.

For the Peak 2 temperature zone transformations, the effect of Fe particles is also negligible.

The analysis of the surface by optical microscopy

Figures 5 to 7 shows the appearance of the sample surfaces after sintering. There can be noted the production of a monolithic base mass in which the particles introduced for reinforcement can be differentiated. The surface profile shown in Figure 5 reveals a correspondence between the size of the particles used and the roughness of the surface.

For all the analysed samples, the presence of open pores is observed on the surface. Their dimensions and shape are correlated with the dimensions of the granular materials in the composite. Depending on how the contact between the particles in the composite is made, the pores may have larger lengths (appearance visible in Figure 6). There is also a rough appearance of their

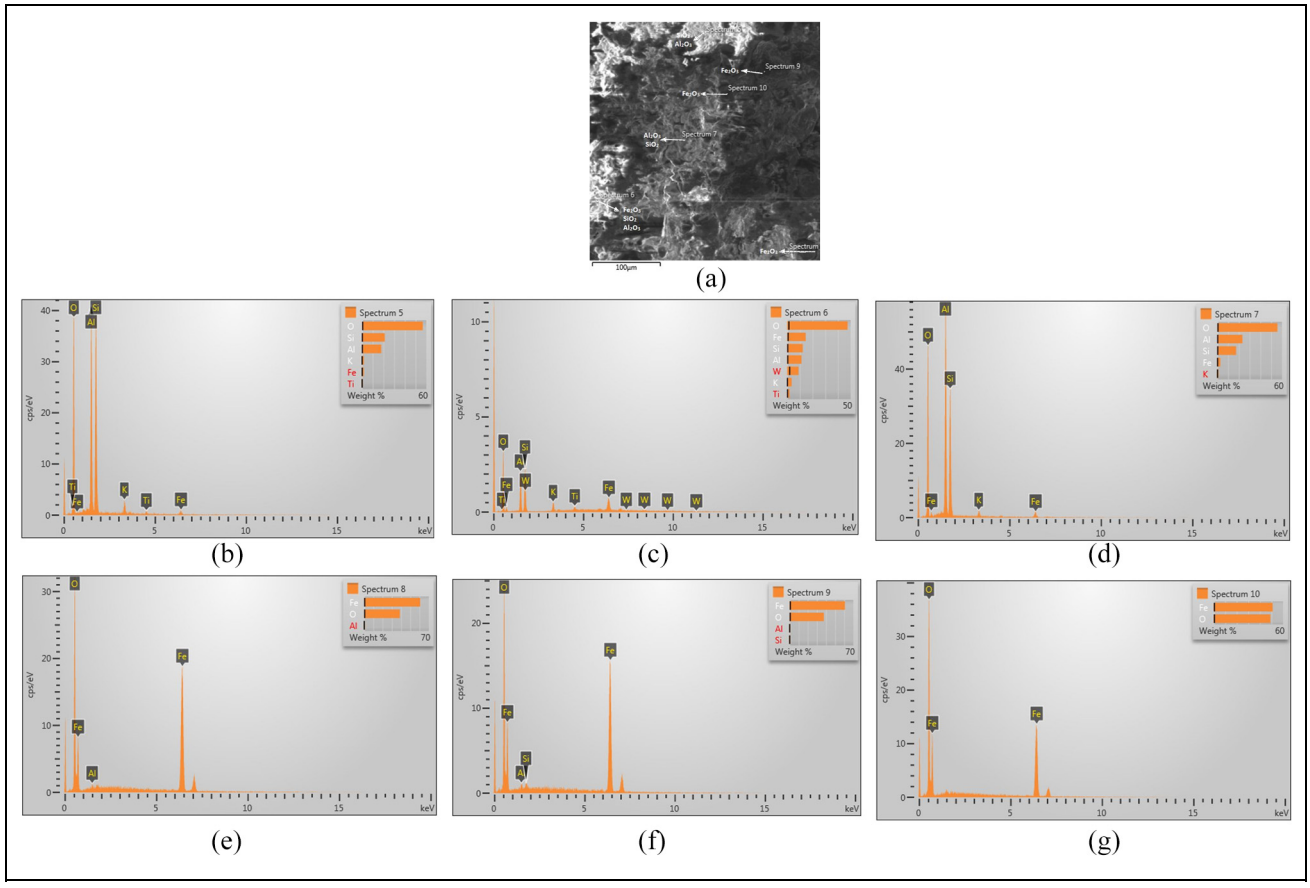

Figure 8. SEM image for the composite with bentonite matrix reinforced with Al_2O_3 and Fe particles: (a) image for the studied area; (b) the chemical composition for the Spectrum 5 area; (c) the chemical composition for the Spectrum 6 area; (d) the chemical composition for the Spectrum 7 area; (e) the chemical composition for the Spectrum 8 area; (f) the chemical composition for the Spectrum 9 area; and (g) the chemical composition for the Spectrum 10 area.

surface, favourable to mechanical retention processes, when using these materials for filtration.

The analysis of the surface by electron microscopy

In addition to highlighting the appearance, as in the case of optical microscopy, the aim was to determine the chemical composition in certain zones to highlight the nature of the materials in such zones. Figures 8 and 9 shows such zones where six local chemical compositions were determined. The chemical composition diagrams allowed the determination of the type of compounds in each case.

There can be noted that in addition to the oxides specific to the ceramic materials used in the preparation of composites, there also occur oxides formed during their sintering, such as iron and aluminium oxides. The oxygen source for such reactions can be both the working atmosphere (at the surface of the materials) as well as the water vapours released from bentonite (a phenomenon highlighted in the differential thermal analyses).

The diffractometric analysis

The composition of these materials includes complex compounds. This is highlighted by the diffraction analyses shown in Figures 10 and 11. They are specific for these materials and have been highlighted in many previous studies.[5–9,43–53] Compared to the basic composition of bentonite, the diffraction analyses highlight the existence of mullite type compound. For the same type of compound there are multiple peaks diffraction angles (respective diffraction angles are specified in Figures 10 and 11).

The diffraction curves also contain compounds introduced into the composite. In the case of the composite with bentonite matrix reinforced with Al_2O_3 and Fe particles, it is more difficult to differentiate Al_2O_3 and the iron oxides from those already existing in the base material (Figure 10).

In the case of the composite with bentonite matrix reinforced with SiC and Al particles, the SiC compound, previously not present, is highlighted (Figure 11).

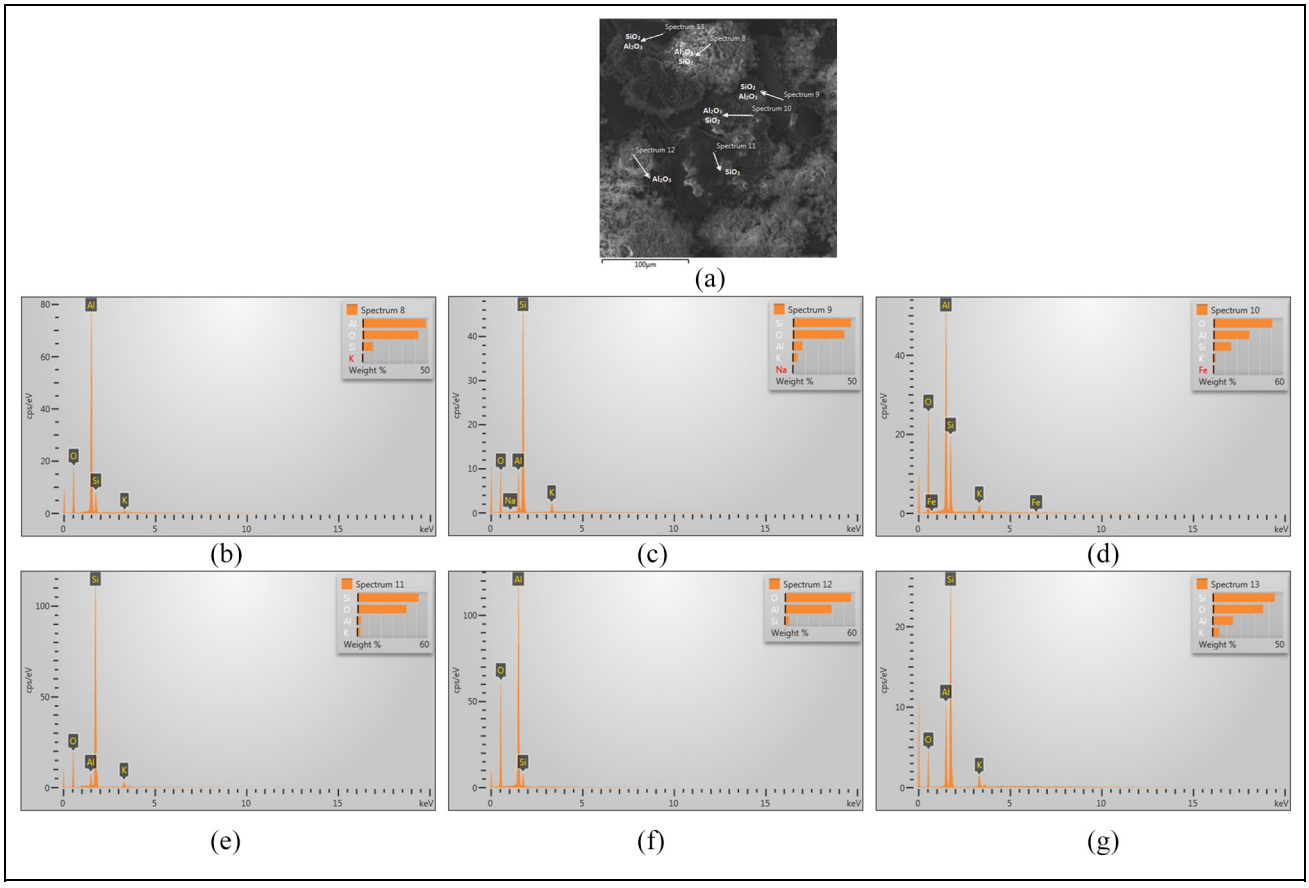

Figure 9. SEM image for the composite with bentonite matrix reinforced with SiC and Al particles: (a) image for the studied area; (b) the chemical composition for the Spectrum 8 area; (c) the chemical composition for the Spectrum 9 area; (d) the chemical composition for the Spectrum 10 area; (e) the chemical composition for the Spectrum 11 area; (f) the chemical composition for the Spectrum 12 area; and (g) the chemical composition for the Spectrum 13 area.

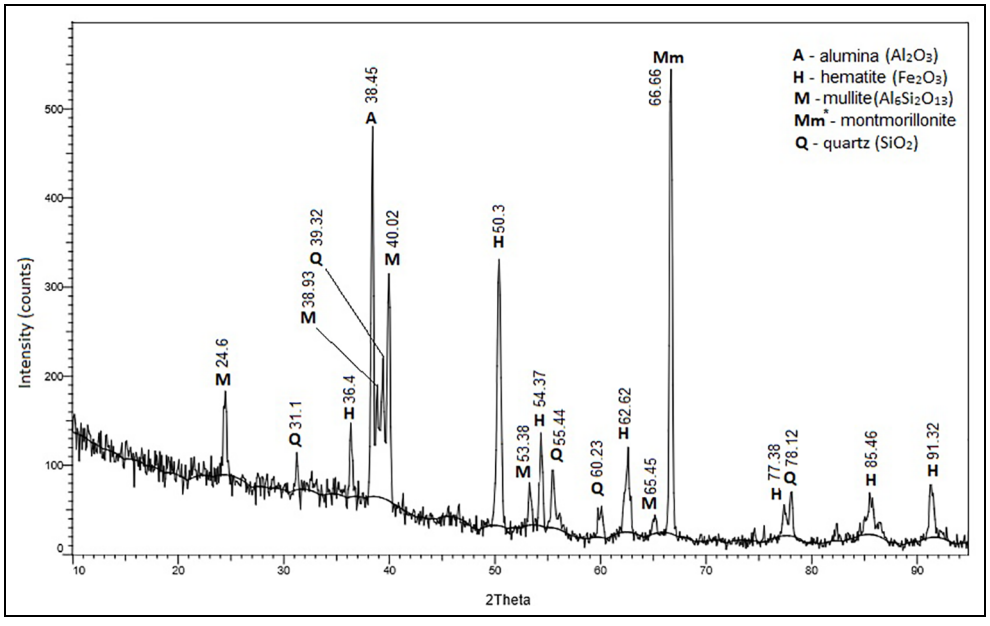

Figure 10. X-ray diffractogram for the composite with bentonite matrix reinforced with Al_2O_3 and Fe particles.
*Identified by the associated presence of the component chemical compounds.

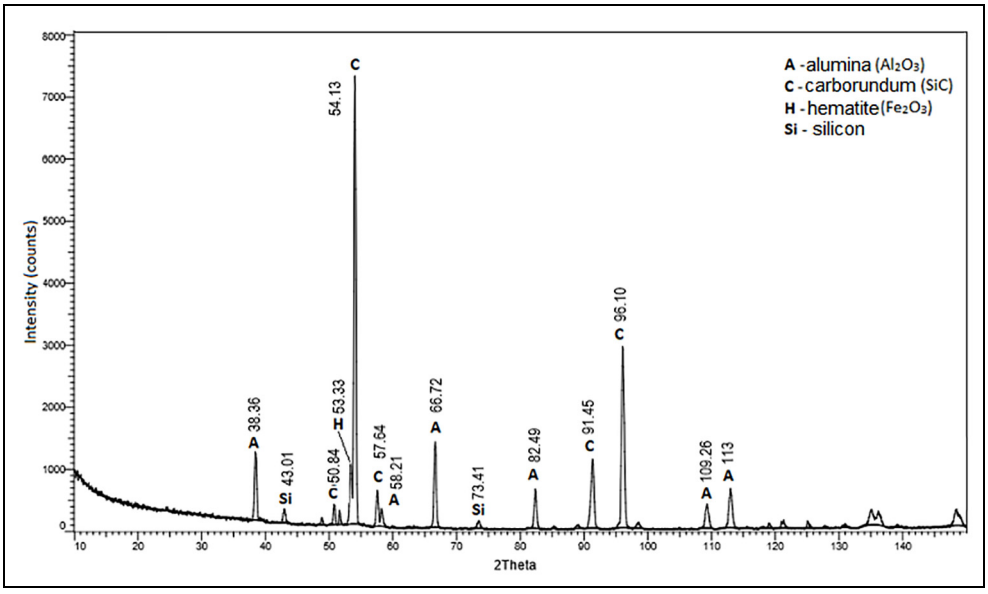

Figure 11. X-ray diffractogram for the composite with bentonite matrix reinforced with SiC and Al particles.

Table 3. Structural characteristic of complex compounds identified by X-ray analysis.

Item	Compound	Crystal lattice type		Crystal lattice parameters					
		System	Space group	*a* (Å)	*b* (Å)	*c* (Å)	α (°)	β (°)	γ (°)
1.	A	Hexagonal	R-3c (167)	4.7602		12.9933	55.27		
2.	H	Hexagonal	R-3c (167)	5.0066		13.6411			
3.	M	Ortho-rhombic	Pbam (55)	7.552	7.6872	2.8843	55.27		
4.	Q	Hexagonal	P3221 (154)	4.9143		5.4058			
5.	C	Cubic	F-43m (216)	4.348			55.27		
6.	Si	Cubic	Fd-3m (227)	5.431			55.27		
7.	Mm	Tetrahedral-ortho-rhombic-tetrahedral							

The analyses did not detect the presence of metals introduced in the form of metallic particles. This is due to their oxidation in the sintering process carried out in the free atmosphere. The resulting oxides (Fe_2O_3 and Al_2O_3) can be identified by diffractometric analysis, without being able to differentiate them from similar compounds in the composite matrix.

The structural characteristic of complex compounds identified by X-ray analysis are presented in Table 3. The crystal lattice parameters identified have values comparable to those in the literature determined under similar conditions.[43–53]

For bentonite-based composites reinforced with Al_2O_3 and Fe particles, the analyses shown in Figure 10, were performed in variant 2θ in the range 10°–95°. The most important phases are hematite, mullite, alumina, quartz and montmorillonite. Hematite (COD 9016457) was identified at 36.4°, 50.3°, 54.37°, 62.62°, 77.38°, 85.46° and 91.32°. It has a hexagonal structure (space group: R-3c (167)) with lattice constant: a = 5.0066 Å and c = 13.6411 Å. Quartz (COD 2100188) is found at 31.1°, 39.32°, 55.44°, 60.23° and 78.12°. It has a hexagonal structure (space group: P3221 (154)) with lattice constant: a = 4.9143 Å and c = 5.4058 Å. Mullite (COD 9010159) was identified at 24.6°, 38.93°, 40.02°, 53.38° and 65.45° and has an orthorhombic structure (space group: Pbam (55)) with lattice constant a = 7.552 Å, b = 7.6872 Å and c = 2.8843 Å. Alumina (COD 9007496) appears at 38.45° and has a hexagonal structure (space group: R-3c (167)) with lattice constant: a = 4.7602 Å and c = 12.9933 Å. Montmorillonite has the most important peak at 66.66° and has a complex lattice: tetrahedral-orthorhombic-tetrahedral. It has identified by the associated presence of the component chemical compounds because in the position of the maximum corresponding to it, several compounds were identified: Fe_2MgO_4, $Al_6Ca_{8.25}Na_{1.5}O_{18}$ and Al_2O_5Si.

For bentonite-based composites reinforced with SiC and Al particles, the analyses shown in Figure 11, were

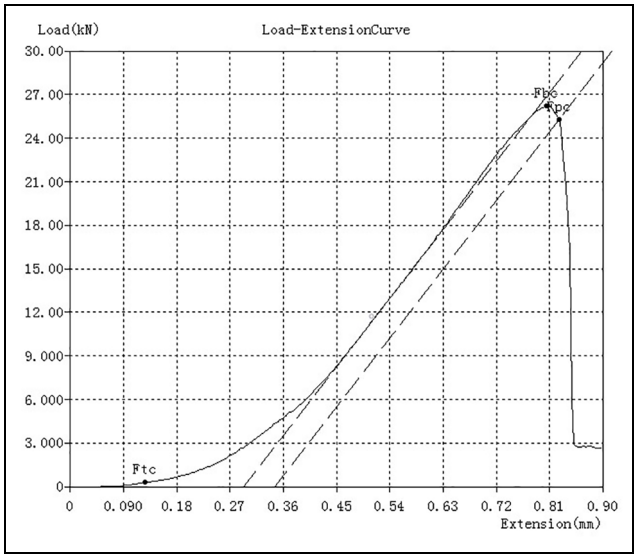

Figure 12. Load-extension curve for the composite with bentonite + Al_2O_3 + 5 wt%Fe.

Table 4. Mechanical properties and porosity for bentonite-based composites.

Sample no.	Compressive strength (MPa)	Pmed porosity (%)
3.1.1.	96	21.22
3.1.1.1.Fe	102	14.78
3.1.1.1.Al	60	14.14
3.1.1.2.Fe	98	7.94
3.1.1.2.Al	64	17.44
3.1.1.3.Fe	46	–
3.1.1.3.Al	94	16.2
3.1.1.4.Al	108	13.95
3.2.1.	109	23.83
3.2.1.1.Fe	116	16.16
3.2.1.1.Al	106	13.57
3.2.1.2.Fe	166	10.31
3.2.1.2.Al	114	14.44
3.2.1.3.Fe	181	10.54
3.2.1.3.Al	129	18.6
3.2.1.4.Fe	215	6.92
3.2.1.4.Al	149	9.82

performed in variant 2θ in the range 10°–150°. The most important phases are alumina, carborundum, hematite and silicon. Alumina is present at 38.36°, 58.21°, 66.72°, 82.49°, 109.26° and 113° and the carborundum at 50.84°, 54.13°, 57.64°, 91.45° and 96.10°. Carborundum (COD 1010995) has a cubic structure (space group: F-43m (216)) with lattice constant: a = 4.348 Å. Hematite is present at 53.33° and silicone at 43.01° and 73.41°. Silicon (COD 2104737) has a cubic structure (space group: Fd-3m (227)) with lattice constant: a = 5.431 Å.

Mechanical properties

For each sample was obtained the load-extension curve. Such a diagram, for the set with bentonite + Al_2O_3 + 5 wt%Fe, is shown in Figure 12. From these diagrams were extracted the specific values that were later used to interpret the results (see Table 4 and Figures 13–16).

For the basic mixture of composites (bentonite + SiC and bentonite + Al_2O_3) the compressive strengths are similar to the results of other previous studies: 88 ± 8 MPa,[3] 63/196 MPa[4] and 70.3 ± 2.8 MPa.[8]

The influence of the metallic particles on the composites mechanical properties is determined by the appearance of their oxides during sintering (in situ process). On the one hand, these oxides can cause a decrease of the properties when they break the bonds in the composite material (when they are different from the composition of the composite matrix – e.g. the addition of Al particles in the bentonite + SiC composite). The effect is visible especially at low values of the addition of

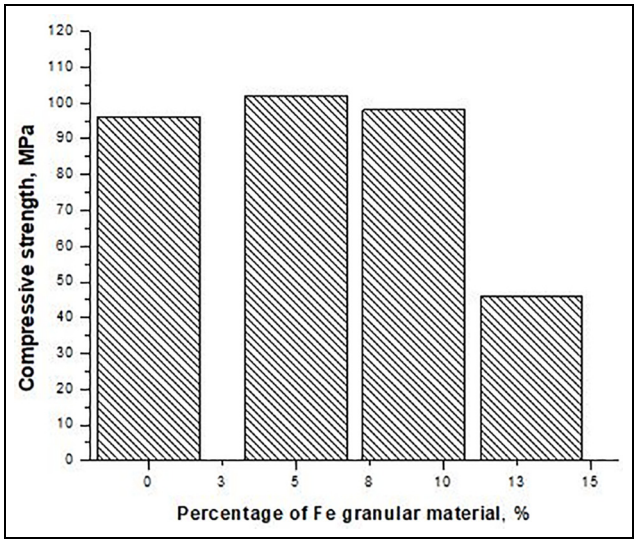

Figure 13. The variation of the compressive strength according to the Fe content for the SiC composite.

metal particles. On the other hand, the formation of oxides is accompanied by a local increase in volume, which causes the compaction of structures and the increase of properties. This effect increases with the amount of metal particles added, as long as the internal stresses that cause the compaction of the materials do not lead to cracks.

For composites with SiC and Fe, the increase of the proportion of Fe powders causes the decrease of the compressive strength. This is due to the fact that the Fe powder oxidizes in the presence of water vapours removed from the matrix during sintering with a

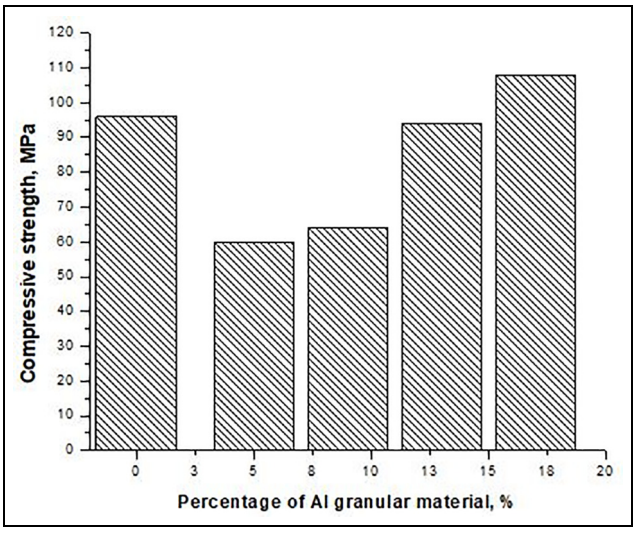

Figure 14. The variation of the compressive strength according to the Al content for the SiC composite.

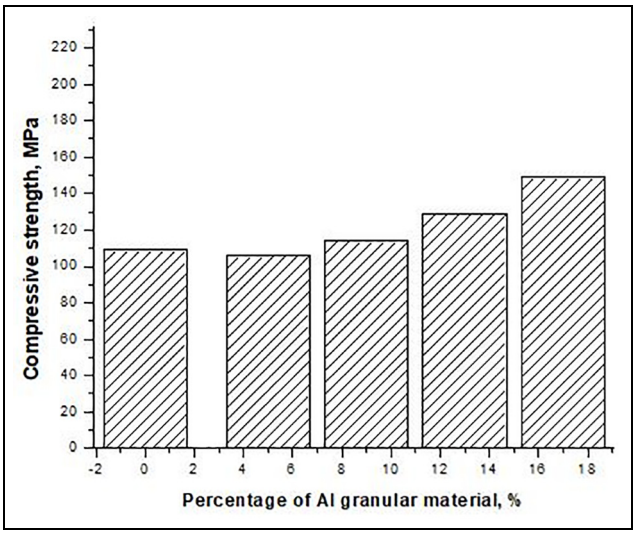

Figure 16. The variation of the compressive strength according to the Al content for the composite with Al_2O_3.

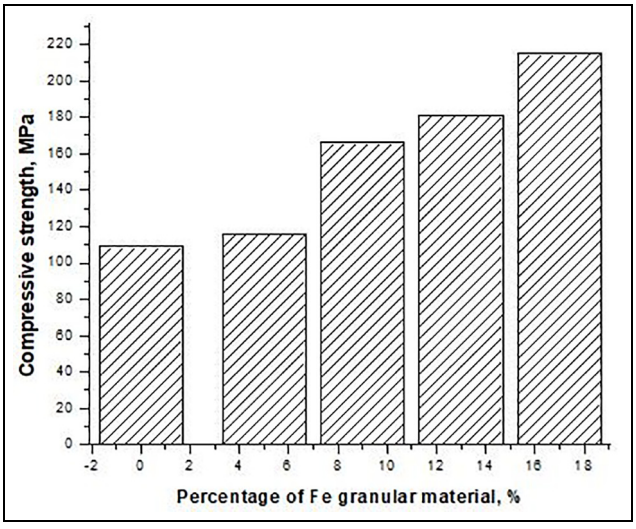

Figure 15. The variation of the compressive strength according to the Fe content for the composite with Al_2O_3.

volume increase which is added to the expansion of the ceramic materials. For a small addition of Fe (less than 9 wt%) the properties increase but not significantly due to the compaction caused by the formation of Fe oxides with increasing volume. To further growth of the particles percentage of Fe significant internal stresses and cracks occur and they reduce the compressive strength. The process is more active near the sample surface (due to O_2 from the atmosphere) but it also occurs in volume (due to O_2 content in the water vapours removed from bentonite). For Fe additions greater than 9 wt%, cracks occur in the samples produced and they substantially reduce the compressive strength.

In all the other cases, the increase of the proportion of metallic powders causes the increase of the compressive strength. There should be noted that the Fe effect changes radically when Al_2O_3 is present in bentonite, compared to when SiC is present in it (see Figure 15 compared to Figure 13). This shows interaction differences between the oxides obtained from the oxidation of Fe particles with SiC and with Al_2O_3, respectively. Basically, as the metallic particles oxidize, the local volume increases induce stresses that relax when the material is sintered by the partial cancellation of the pores, causing the increase of the compressive strength as long as no cracks occur in the material. The higher SiC hardness does not allow a good distribution in the material of these stresses and thus, starting with higher percentages of Fe particles, the cracks begin to occur and the mechanical properties decrease (the case of the bentonite + SiC + Fe particles mixture). The best compressive strength of the studied materials was obtained for the mixture bentonite + Al_2O_3 + 17% Fe particles (see Figure 15).

And in the case of Al metallic particles, a different behaviour was observed between the composites with SiC and Al_2O_3 particles (Figure 14 compared to Figure 16). In the first case, after a strong decrease of the compressive strength, follows an important increase of it until the specific values of the matrix are exceeded (bentonite + SiC). The behaviour is determined as in the case of Fe particles by the oxidation of Al particles and the role that these oxides have on the material. At small additions of Al particles, the amount of oxides can interrupt intragranular bonds in the composite without causing, at the same time, the compaction of the material due to the increase in volume given by Al_2O_3. With increasing percentage of Al, the

compaction process is accentuated and consequently the compressive strength increases. It should be noted that, on these samples, within the limits of the studied compositions, the presence of cracks was not observed (Figure 14). In the case of composites with bentonite and Al_2O_3 (Figure 16), the effect of adding Al particles is to increase the properties explained by the compaction effect of the structure during sintering.

The compressive strengths are high enough to preserve the geometry and dimensions of the finished products during processing and use. They are comparable to those of materials presented in similar studies.[54]

The porosity

This one was determined by measuring the volume of the open pores. The samples were immersed in a volume of water V0 from a graduated cylinder, and the volume V1 was read immediately. Volume V2 was read after holding the sample for 30 min in water, and then the sample was extracted and volume V3 of the water left in the cylinder was read. The following expressions were used for the actual calculation:

$$P1 = \frac{V0 - V3}{V1 - V0}100, \quad (2)$$

$$P2 = \frac{V1 - V2}{V1 - V0}100, \quad (3)$$

Table 4 and Figures 17 and 18 presents the values of the porosities thus determined, as averages between at least six samples from the same category of materials. The expressions 1 and 2 were used simultaneously for mutual verification. As shown in Figures 17 and 18, the porosity values are higher in the case of the basic mixtures: bentonite + SiC (21.22%) and bentonite + Al_2O_3 (23.83%). These values are similar to those obtained in previous research[4,8,9] and decrease with the increase of the percentage of metallic powders added in them. The decrease is higher in the case of adding Fe powders than of adding Al. This influence is the result of oxidation of metal powders during sintering accompanied by volume increases and pore shrinkage in the material. The results are naturally correlated with those regarding the compressive strength of the studied materials. The shape of the pores in these materials is also very important. The observations on the surface by optical microscopy reveal pores with very varied dimensions between 10 and 150 μm (such pores can be seen in Figure 19). Average pore diameter of 23.94 μm is within comparable limits with previous studies on similar materials.[4]

Open pores have irregular shapes, sometimes acicular (especially in the case of materials with larger additions of metal powders). This appearance (can also be seen in Figures 6–9) is an advantage for the use of these materials in filtration processes. At the same time, there is noted that the addition of metal powders is a way to control the filtration characteristics.

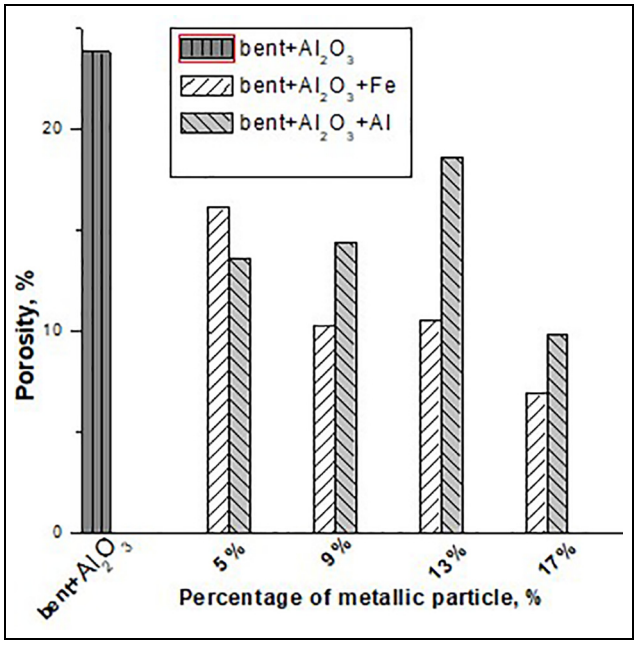

Figure 17. The variation of the porosity according to the metallic particle for the composite with Al_2O_3.

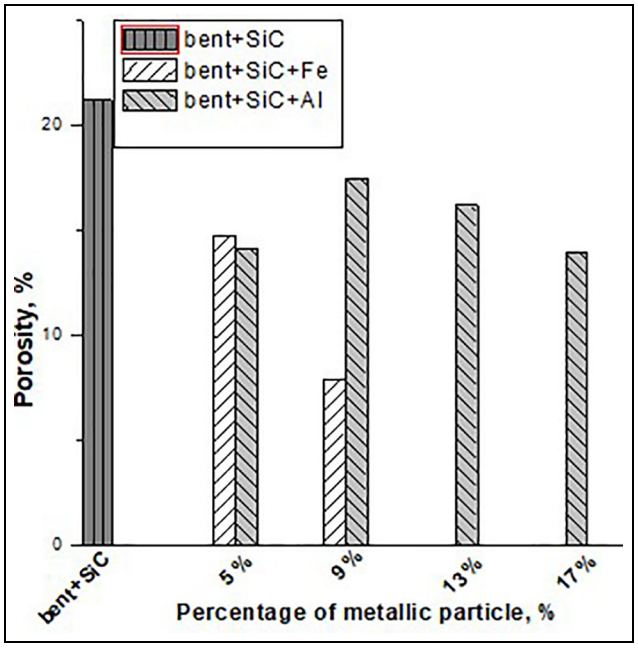

Figure 18. The variation of the porosity according to the metallic particle for the composite with SiC.

Conclusions

In order to establish a correct procedure (technology) for the production of bentonite-based composites, it is

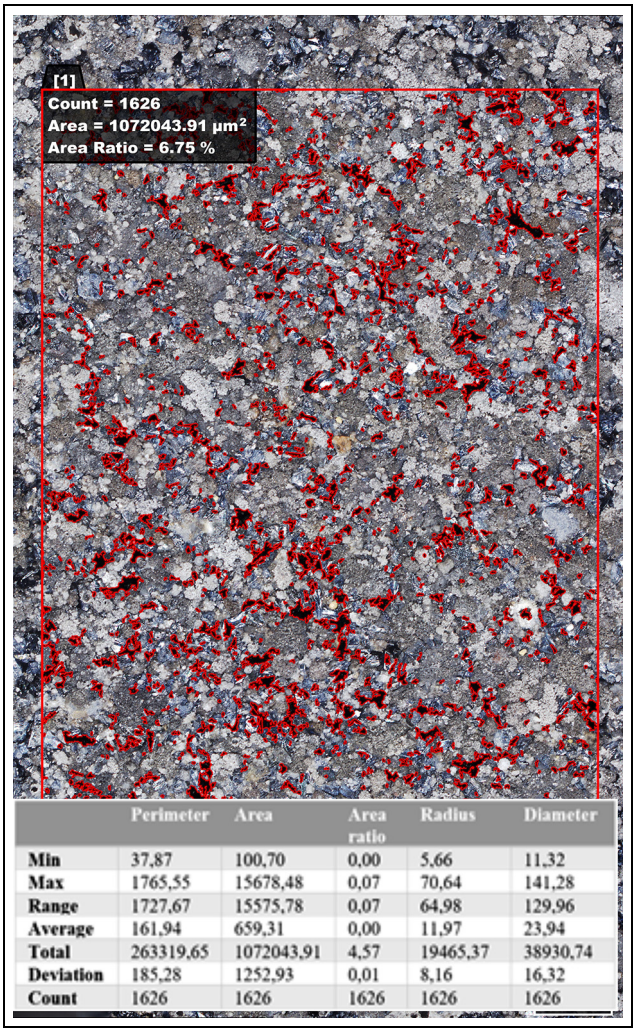

	Perimeter	Area	Area ratio	Radius	Diameter
Min	37,87	100,70	0,00	5,66	11,32
Max	1765,55	15678,48	0,07	70,64	141,28
Range	1727,67	15575,78	0,07	64,98	129,96
Average	161,94	659,31	0,00	11,97	23,94
Total	263319,65	1072043,91	4,57	19465,37	38930,74
Deviation	185,28	1252,93	0,01	8,16	16,32
Count	1626	1626	1626	1626	1626

Figure 19. The appearance of open pores on the surface of the sample made of composite material based on bentonite reinforced with matrix of SiC and Al (sample 3.1.1.4.Al from Table 1).

necessary to know in detail its transformations when heating for sintering, respectively the effects that the reinforcement materials have on these transformations. The thermal analyses (dilatometry and differential thermal analysis) used in the present study highlighted the dimensional, mass and caloric variations, which occur in well-defined temperature ranges for bentonite (80°C–300°C and 500°C–600°C). The addition of ceramic powders of SiC and Al_2O_3 does not significantly influence the bentonite transformations in these thermal ranges. Metallic powders of Al and Fe have important influences that are highlighted especially by differential thermal analysis. These influences are due to the chemical interactions between these elements and the water in the mixture, the ceramic powders in the mixture, the oxygen in the sintering atmosphere, respectively the melting of the powder (in the case of Al). Within the studied compositions and of the applied sintering method (in the oven atmosphere) the metallic powders are completely transformed. This reality (objective pursued) was highlighted by X-ray diffractometry analyses and SEM-EDX electron microscopy analyses, in which, in the composites made, the presence of Al and Fe metal particles was not found after sintering.

Ceramic powders of SiC and Al_2O_3 type are needed in bentonites-based composites to obtain porous structures. The addition of metallic Fe and Al powders provided both an improvement of the mechanical properties (increases in the compressive strength) and a control of the pore size and shape. SiC is more active than Al_2O_3 in relation to the metallic powders of Fe and Si determining limits of concentrations in the case of Fe (recommended max. 9 wt% Fe in association with SiC compared to 17 wt% Fe in association with Al_2O_3).

The compressive strengths increase with the increase of the percentages of added metal powders, due to the compaction of the materials at sintering as a result of the formation of Fe and Al compounds (in the reactions mentioned above). The combination of Al_2O_3 with Fe and Al powders ensures compressive strengths higher than the association of SiC with Fe and Al powders with the same compositions. The highest compressive strengths were achieved for Al_2O_3 composites and an addition of 17 wt% Fe (215 MPa).

By compacting of the material to sintering, its porosity decreases. This decrease is even greater as the proportion of metal powders in composites is higher. Also, it is more pronounced in the case of Fe than in the case of Al. At the same time, the shape of the pores changes depending on the place and the possibilities of growth of Fe and Al compounds during sintering (fact shown by the study by optical microscopy). This is the way to control the filtering capacity of these composites.

Acknowledgements

We hereby acknowledge the structural founds project PRODD (POS-CCEO.2.2.1.ID 123SMIS 2637ctr. No 11/2009) for providing the infrastructure used in this work and the project SOP HRD, ID137070 financed from the European Social Fund and by the Romanian Government.

Declaration of conflicting interests

The author(s) declared no potential conflicts of interest with respect to the research, authorship, and/or publication of this article.

Funding

The author(s) received no financial support for the research, authorship, and/or publication of this article.

ORCID iD

Simona Matei https://orcid.org/0000-0002-8040-9409

References

1. Deckers J, Vleugels J and Kruth JP. Additive manufacturing of ceramics: a review. *J Ceram Sci Technol* 2014; 5: 245–260.
2. Schnieder J, Lynen L, Traon N, et al. Crack formation and shape of fracture surface in tabular-alumina-based castables with addition of specific aggregates. *J Ceram Sci Technol* 2014; 5: 131–136.
3. Bohm A, Aneziris CG and Malzbender J. Dependent thermo-mechanical behavior of novel alumina-based refractories. *J Ceram Sci Technol* 2014; 5: 167–171.
4. Choi HJ, Kim JU, Kim SH, et al. Preparation of granular ceramic filter and prediction of its collection efficiency. *Aerosol Sci Technol* 2014; 48: 1070–1079.
5. Pastila P, Helanti V, Nikkilä AP, et al. Environmental effects on microstructure and strength of SiC-based hot gas filters. *J Eur Ceram Soc* 2001; 21: 1261–1268.
6. Alvin MA. Advanced ceramic materials for use in high-temperature particulate removal systems. *Ind Eng Chem Res* 1996; 35: 3384–3398.
7. Shi Y, Meng Y, Chen D, et al. Highly ordered mesoporous silicon carbide ceramics with large surface areas and high stability. *Adv Funct Mater* 2006; 16: 561–567.
8. Liu S, Zeng YP and Jiang D. Fabrication and characterization of cordierite-bonded porous SiC ceramics. *Ceram Int* 2009; 35: 597–602.
9. Li J, Lin H and Li J. Factors that influence the flexural strength of SiC-based porous ceramics used for hot gas filter support. *J Eur Ceram Soc* 2011; 31: 825–831.
10. Şan O, Abalı S and Hoşten Ç. Fabrication of microporous ceramics from ceramic powders of quartz–natural zeolite mixtures. *Ceram Int* 2003; 29: 927–931.
11. Ivanets AI, Rat'ko AI, Azarova TA, et al. Preparation and properties of microfiltration membranes based on natural crystalline SiO_2. *Ceram Int* 2014; 40: 12343–12351.
12. Al-Otoom AY, Ninomiya Y, Moghtaderi B, et al. Coal ash buildup on ceramic filters in a hot gas filtration system. *Energy Fuels* 2003; 17: 316–320.
13. Şan O, Gören R and Özgür C. Purification of diatomite powder by acid leaching for use in fabrication of porous ceramics. *Int J Miner Process* 2009; 93: 6–10.
14. Chaim R, Levin M, Shlayer A, et al. Sintering and densification of nanocrystalline ceramic oxide powders: a review. *Adv Appl Ceram* 2008; 107: 159–169.
15. Zhou J, Fan JP, Sun GL, et al. Preparation and properties of porous silicon nitride ceramics with uniform spherical pores by improved pore-forming agent method. *J Alloys Comp* 2015; 632: 655–660.
16. Lin H, Sun J, Li C, et al. A facile route to synthesize WC–Co nanocomposite powders and properties of sintered bulk. *J Alloys Comp* 2016; 682: 531–536.
17. Tiunova OV, Zadorozhnaya OY, Nepochatov YK, et al. Ceramic membranes based on scandium-stabilized ZrO2 obtained by tape casting technique. *Russ J Electrochem* 2014; 50: 719–724.
18. Ghouil B, Harabi A, Bouzerara F, et al. Development and characterization of tubular composite ceramic membranes using natural alumino-silicates for microfiltration applications. *Mater Charact* 2015; 103: 18–27.
19. Ivanets AI, Prozorovich VG, Kouznetsova TF, et al. Mesoporous manganese oxides prepared by sol-gel method: synthesis, characterization and sorption properties towards strontium ions. *Environ Nanotechnol Monitor Manag* 2016; 6: 261–269.
20. Yarovaya OV, Lemeshev DO, Mostovaya UL, et al. Production of flat ceramic membrane contactors with a catalytically active layer based on Co_3O_4. *Glass Ceram* 2016; 73: 19–21.
21. Özgür C and Şan O. Slip cast forming of multilayer ceramic filter by fine particles migration. *Ceram Int* 2008; 34: 1935–1939.
22. Islam MF, Rizvi MH, Khan TA, et al. Development of ceramic candle filters by slip casting process. *Key Eng Mater* 2014; 608: 85–90.
23. Han IS, Seo DW, Kim SY, et al. Fabrication and properties of SiC candle filter by vacuum extrusion and ramming process(II). *J Korean Ceram Soc* 2010; 467: 515–523.
24. Hwang SS, Park SW, Han JH, et al. Reaction bonded SiC hot gas filter using Si-melting filtration techniques. *Key Eng Mater* 2005; 287: 177–182.
25. Uddin MK. A review on the adsorption of heavy metals by clay minerals, with special focus on the past decade. *Chem Eng J* 2017; 308: 438–462.
26. Bouzerara F, Harabi A, Achour S, et al. Porous ceramic supports for membranes prepared from kaolin and doloma mixtures. *J Eur Ceram Soc* 2006; 26: 1663–1671.
27. Masmoudi S, Larbot A, Feki HE, et al. Elaboration and characterisation of apatite based mineral supports for microfiltration and ultrafiltration membranes. *Ceram Int* 2007; 33: 337–344.
28. Saffaj N, Alami-Younssi S, Albizane A, et al. Elaboration and properties of TiO2–ZnAl2O4 ultrafiltration membranes deposited on cordierite support. *Sep Purif Technol* 2004; 36: 107–114.
29. Saffaj N, Persin M, Alami-Younssi S, et al. Removal of salts and dyes by low ZnAl2O4–TiO2 ultrafiltration membrane deposited on support made from raw clay. *Sep Purif Technol* 2005; 47: 36–42.
30. Saffaj N, Persin M, Alami-Younssi S, et al. Elaboration and characterization of microfiltration and ultrafiltration membranes deposited on raw support prepared from natural Moroccan clay: application to filtration of solution containing dyes and salts. *Appl Clay Sci* 2006; 31: 110–119.
31. Archiou B, Elomari H, Ouammou M, et al. Elaboration and characterization of flat ceramic microfiltration membrane made from natural Moroccan pozzolan (Central Middle Atlas). *J Mater Environ Sci* 2016; 7: 196–204.
32. Şan O and Hoşten Ç. Filtration testing of a ceramic capillary filter produced from a high-silica glaze. *Miner Eng* 2002; 15: 553–556.
33. Fei Y, Huang CH and Liu H. The phase composition and mechanical properties of Al2O3-TiN-TiC ceramic materials with different Ni content. *J Ceram Sci Technol* 2019; 10: 1–8.

34. Ma Y, Li J, Wang X, et al. Highly permeable macroporous cordierite ceramics with controlled microstructure produced by particle-stabilized emulsions with a reactive thermal treatment. *J Eur Ceram Soc* 2017; 37: 3203–3211.
35. Rhodes D. *Clay and glazes for the potter*. Eastford, CT: Martino Fine Books, 2015.
36. Ulbricht M. Advanced functional polymer membranes. *Polymer* 2006; 47: 2217–2262.
37. Bernardo P, Drioli E and Golemme G. Membrane gas separation: a review/state of the art. *Ind Eng Chem Res* 2009; 48: 4638–4663.
38. Ayari F, Srasra E and Trabelsi-Ayadi M. Characterization of bentonitic clays and their use as adsorbent. *Desalination* 2005; 185: 391–397.
39. Holzer L, Münch B, Rizzi M, et al. 3D-microstructure analysis of hydrated bentonite with cryo-stabilized pore water. *Appl Clay Sci* 2010; 47: 330–342.
40. Park KH, Sung IK and Kim DP. A facile route to prepare high surface area mesoporous SiC from SiO2 sphere templates. *J Mater Chem* 2004; 14: 3436.
41. Jin GQ and Guo XY. Synthesis and characterization of mesoporous silicon carbide. *Microporous Mesoporous Mater* 2003; 60: 207–212.
42. Liu Z, Shen W, Bu W, et al. Low-temperature formation of nanocrystalline β-SiC with high surface area and mesoporosity via reaction of mesoporous carbon and silicon powder. *Microporous Mesoporous Mater* 2005; 82: 137–145.
43. Zhirong L, Azhar Uddin M and Zhanxue S. FT-IR and XRD analysis of natural Na-bentonite and Cu(II)-loaded Na-bentonite. *Spectrochim Acta A Mol Biomol Spectrosc* 2011; 79: 1013–1016.
44. Pentrák M, Hronský V, Pálková H, et al. Alteration of fine fraction of bentonite from Kopernica (Slovakia) under acid treatment: a combined XRD, FTIR, MAS NMR and AES study. *Appl Clay Sci* 2018; 163: 204–213.
45. Ghadr S and Assadi-Langroudi A. Structure-based hydro-mechanical properties of sand-bentonite composites. *Eng Geol* 2018; 235: 53–63.
46. Sainz MA, Serrano FJ, Amigo JM, et al. XRD microstructural analysis of mullites obtained from kaolinite–alumina mixtures. *J Eur Ceram Soc* 2000; 20: 403–412.
47. Ahmed A, Chaker Y, Belarbi EH, et al. XRD and ATR/FTIR investigations of various montmorillonite clays modified by monocationic and dicationic imidazolium ionic liquids. *J Mol Struct* 2018; 1173: 653–664.
48. Sun Z, Park Y, Zheng S, et al. XRD, TEM and thermal analysis of Arizona Ca-montmorillonites modified with didodecyldimethylammonium bromide. *J Colloid Interface Sci* 2013; 408: 75–81.
49. Bochenek D, Niemiec P, Korzekwa J, et al. Microstructure and properties of the ferroelectric-ferromagnetic PLZT-ferrite composites. *Symmetry* 2018; 10: 59.
50. Fouad DE, Zhang C, El-Didamony H, et al. Improved size, morphology and crystallinity of hematite (α-Fe2O3) nanoparticles synthesized via the precipitation route using ferric sulfate precursor. *Results Phys* 2019; 12: 1253–1261.
51. Suriyanarayanan N, Nithin KVK and Bernardo E. Mullite glass ceramics production from coal ash and alumina by high temperature plasma. *J Non-Oxide Glasses* 2009; 1: 247–260.
52. Chen H, Jiang J and Zhao H. Synthesis of highly dispersed silicon carbide powders by a solvothermal-assisted sol–gel process. *Appl Phys A* 2018; 124: 470.
53. Wang MS and Fan LZ. Silicon/carbon nanocomposite pyrolyzed from phenolic resin as anode materials for lithium-ion batteries. *J Power Sources* 2013; 244: 570–574.
54. Durowaye SI, Sekunowo OI, Lawal AI, et al. Development and characterisation of iron millscale particle reinforced ceramic matrix composite. *J Taibah Univ Sci* 2017; 11: 634–644.